Electroreduction of Dioctadecylviologen in a Self-Assembled Phospholipid Monolayer on Mercury and Its Role as an Electron Mediator

Roberto Herrero,[†] Maria Rosa Moncelli, Lucia Becucci, and Rolando Guidelli*

Chemistry Department, University of Florence, Via G. Capponi, 9, 50121-Florence, Italy

Received: August 8, 1996; In Final Form: December 29, 1996[⊗]

The electroreduction mechanism of dioctadecylviologen (V^{2+}) incorporated in a self-assembled dioleoylphosphatidylcholine (DOPC) monolayer supported on a mercury electrode has been investigated in aqueous 0.1 M KCl by chronocoulometry and other electrochemical techniques. V^{2+} is reduced in two consecutive charge steps, $2V^{2+} + 3e \rightarrow V_2^+$ and $V_2^+ + e \rightarrow 2V^0$, involving 3/2 and 1/2 of a Faraday per mole of reactant, respectively. Both charge steps are exclusively controlled by the rate of the elementary coupling step $V^+ + V^0 \rightarrow V_2^+$. V^{2+} acts as an electron transfer mediator from $Fe(CN)_6^{3-}$ dissolved in the aqueous solution to the mercury surface across the DOPC monolayer, which is impermeable to $Fe(CN)_6^{3-}$ in the absence of V^{2+}. This mediation takes place only along the first charge step, $2V^{2+} + 3e \rightarrow V_2^+$ and increases with the V^{2+} concentration in the lipid monolayer less than proportionally; this behavior points to the radical cation V^+ as the electron transfer mediator from the mercury surface to the aqueous ferricyanide.

Introduction

Viologens have been extensively investigated in the literature because their well-behaved electrochemistry has led to their use in a variety of studies, including electron transfer mediation to various biological molecules,[1−9] surface-enhanced Raman studies of adsorption at electrode surfaces,[10−12] behavior of supramolecular assemblies at electrode surfaces,[13−16] and applications for electrochromic display devices.[17,18]

Viologens exist in three main oxidation states, namely,

$$V^{2+} \overset{E'_0}{\longleftrightarrow} V^{\bullet+} \overset{E''_0}{\longleftrightarrow} V^0$$

The first reduction step is highly reversible and can be cycled many times without significant side reactions. The further reduction to the fully reduced state is normally less reversible, because V^0 is frequently insoluble and gives rise to adsorption[10] and/or precipitation phenomena on the electrode surface.[19−23] The redox potentials E'_0 and E''_0 depend on solvent, substituent radicals, anion, and temperature.

Four main approaches have been used to investigate these systems: (i) self-assembly of amphiphilic viologens containing sufficiently long alkyl chains on electrode surfaces from their dilute solutions;[24−29] (ii) immobilization of the viologen redox moiety on the electrode surface by derivatizing it with alkyl chains containing −SH groups anchoring the compound to the electrode[30] or with groups that polymerize on the electrode surface;[31−33] (iii) Langmuir−Blodgett transfer of amphiphilic viologens from the air/solution interface to the electrode/solution interface;[10,14,34] (iv) solubilization of the viologen redox moiety derivatized with alkyl substituents in vesicles prepared from natural lipid components or synthetic surfactants.[35−44]

Incorporation of amphiphilic viologens in a matrix impermeable to hydrophilic ions provides a mean for elucidating the mechanism by which these compounds mediate electron transfer across the matrix. The use of unilamellar vesicles is attractive, but the interpretation of results is complicated by the fact that translocation of charged species across vesicles is associated with the development of a transmembrane potential that may notably affect the reaction kinetics; this may explain why there is no general consensus on the mechanism of electron mediation by viologen derivatives across vesicles.[39−44] In principle, planar lipid mono-, bi-, or multilayers interposed between an aqueous and a metal phase, or else lipid bilayers interposed between two aqueous solutions, may allow a control of the transmembrane potential, thus simplifying experimental conditions and facilitating the singling out of the species directly responsible for electron mediation. $C_{18}C_2V^{2+}$ was actually incorporated in a lipid matrix about 3.7 μm thick, obtained by evaporating a solution of phosphatidylcholine and $(C_{18}C_2V^{2+})$-Br_2 in chloroform on the tip of a glassy carbon electrode:[45] cyclic voltammograms corresponding to the stepwise reduction of $C_{18}C_2V^{2+}$ to $C_{18}C_2V^+$ and $C_{18}C_2V^0$ and to the subsequent reoxidation were obtained. Unfortunately, the poorly defined organization of the lipid multilayer makes a kinetic investigation of the mechanism of electron mediation inside this lipid matrix hardly feasible.

This paper reports an investigation on the mechanism of electroreduction of dioctadecylviologen, $(C_{18})_2V^{2+}$ (henceforth briefly denoted by V^{2+}), incorporated in a self-assembled dioleoylphosphatidylcholine (DOPC) monolayer supported by mercury and on its role as an electron transfer mediator from aqueous ferricyanide to the electrode across the monolayer. The choice of this viologen derivative is justified by its having two alkyl chains whose length matches that of the hydrocarbon tails of DOPC; this facilitates its intercalation in the lipid monolayer. The phospholipid coating was obtained by spreading a solution of DOPC in pentane on the surface of an aqueous electrolyte, allowing the solvent to evaporate, and immersing a hanging mercury drop electrode in the electrolyte. This procedure gives rise to half a bilayer, with the hydrocarbon tails directed toward the hydrophobic mercury surface and the polar heads directed toward the solution. The use of a lipid-coated mercury electrode as a biomimetic membrane was introduced by Miller[46] and subsequently adopted in a modified version by Nelson.[47] The defect-free support to the lipid film provided by liquid mercury and the complete absence of pentane in the film impart to the film high mechanical stability, resistance to electric fields, and reproducibility, which are not shared by planar black lipid membranes. By an accurate design of the stationary electrode

[†] On leave from University of La Coruña (Spain).

[⊗] Abstract published in *Advance ACS Abstracts,* March 1, 1997.

S1089-5647(96)02407-8 CCC: $14.00

and of the electrolysis cell, it was therefore possible to determine the intrinsic p*K* values of the ionizable groups of DOPC, phosphatidylethanolamine, phosphatidylserine (PS),[48] and phosphatidic acid,[49] the adsorption coefficients of tetraphenylphosphonium and tetraphenylborate ions in DOPC and PS monolayers,[50] and the mechanism of electroreduction of ubiquinone-10 in a DOPC monolayer.[51]

Experimental Section

The water used was obtained from light mineral water by distilling it once and by then distilling the water so obtained from alkaline permanganate, while constantly discarding the heads. Merck reagent grade KCl was baked at 500 °C before use to remove any organic impurities. DOPC was obtained from Lipid Products (South Nutfield, Surrey, England). Dioctadecylviologen (V^{2+}) bromide was kindly provided by Prof. D. Schiffrin (University of Liverpool) and was used without further purification. $V^{2+}Br_2$ was dissolved in a 4/1 (v/v) mixture of chloroform and ethanol and stored at room temperature in dark bottles to avoid any alteration due to a long exposure to light. Working solutions of DOPC + V^{2+} in pentane for spreading on the surface of the aqueous electrolyte in the cell were prepared every third day and stored at −20 °C. All measurements were carried out in aqueous 0.1 M KCl at 25 °C. Before spreading the pentane solution the aqueous electrolyte was deaerated with argon, which was kept flowing in the cell over the solution during measurements.

The homemade hanging mercury drop electrode (HMDE) employed in the measurements, the cell, and the detailed procedure to coat the HMDE with a self-assembled lipid monolayer are described elsewhere.[48,49] All potentials were measured versus a saturated calomel electrode (SCE). Normal and differential pulse polarographic measurements as well as differential capacity measurements were carried out using a Metrohm Polarecord E506 (Herisau, Switzerland). In differential capacity measurements the ac signal had a 10 mV amplitude and a 75 Hz frequency; the system was calibrated using a precision capacitor. Cyclic voltammetric measurements were carried out with an Amel Model 473 polarographic analyzer (Milano, Italy).

A chronocoulometric procedure described elsewhere,[52] which made use of a wholly computerized apparatus, was employed. The microprocessor used to control all the operations was a Model NOVA 4X from Data General (Westboro, MA), whereas an Amel Model 551 (Milano, Italy) fast rise potentiostat with a 0.1 μs rise time was employed for the potentiostatic control of the three-electrode system. The detailed scheme of the homemade electronic current integrator working under microprocessor control is described in ref 53.

Each chronocoulomogram consisted of a series of consecutive potential jumps of progressively increasing height from a fixed initial value E_i, which was set equal to −0.2 V, to different final values E ranging from −0.2 to −0.7 V, and was recorded on a single lipid-coated mercury drop. The charge $Q(t)$ following each potential jump $E_i \rightarrow E$ was recorded versus the time t elapsed from the instant of the jump for 100 ms, after which the potential was stepped back to E_i, where it remained for 3 s. During this period the reduction product of V^{2+} was completely reconverted to V^{2+}. Thus, an increase in the rest time at E_i beyond 3 s left the charge $Q(t)$ practically unaltered. Curves of the differential capacity C of the phospholipid monolayer deposited on mercury were constantly measured against the applied potential E after recording each chronocoulomogram.

The charge density σ_M on the lipid-coated mercury drop at constant applied potential was estimated by contracting the drop surface by an accurately measured amount while keeping its neck in contact with the DOPC + V^{2+} layer at the argon/electrolyte interface and by recording the charge flowing along the external circuit as a consequence of this contraction.[54]

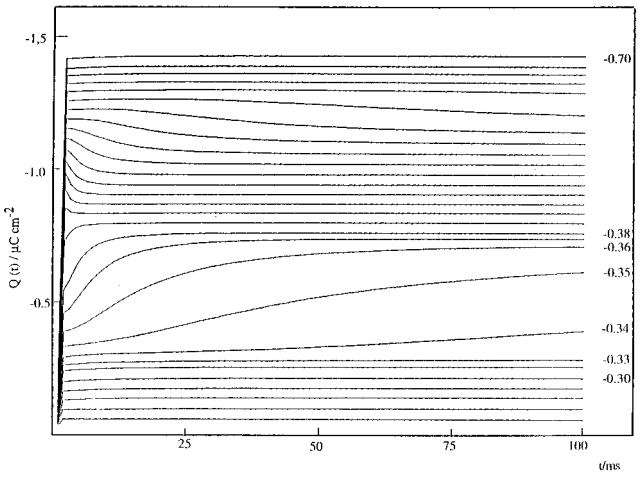

Figure 1. $Q(t)$ versus t curves for the electroreduction in aqueous 0.1 M KCl of 2 mol % V^{2+} incorporated in a self-assembled DOPC monolayer deposited on mercury. The curves were obtained by stepping the potential from a fixed initial value $E_i = -0.200$ V to final values E varying from −0.220 to −0.700 V. From bottom to top, the E values are −0.22, −0.24, −0.26, −0.28, −0.30, −0.32, −0.33, −0.34, −0.35, −0.36, −0.37, −0.38, −0.40, −0.42, −0.44, −0.46, −0.48, −0.50, −0.52, −0.54, −0.56, −0.58, −0.60, −0.62, −0.64, −0.66, −0.68, and −0.70 V/SCE.

Results

Figure 1 shows a series of curves of the charge $Q(t)$ following the potential jump −0.2 V → E as a function of time t elapsed from the instant of the jump, for several final potentials E: the curves refer to a DOPC monolayer containing 2 mol % V^{2+}. At the less negative E values at which the viologen is still electroinactive, the charge $Q(t)$ increases abruptly in less than 1 ms, because of the flow of the capacitive current that is required to charge the interphase, and then attains a time independent value. At more negative E values $Q(t)$ increases in time first abruptly, due to the capacitive contribution, and then more slowly, due to the gradual electroreduction of V^{2+} in time. As E becomes progressively more negative, the rate of V^{2+} electroreduction increases very rapidly, until all V^{2+} incorporated in the lipid monolayer is reduced in less than 1 ms, after which the charge $Q(t)$ attains once again a time independent value. With a further negative shift of E the charge $Q(t)$ decreases in time first rapidly and then more slowly and to a lower extent, until ultimately the charge $Q(t)$ becomes once again independent of time. The decrease of $Q(t)$ in time is quite unusual, because it corresponds to the flow of an anodic current following a negative potential jump.

Figure 2 shows a series of curves of $Q(t{=}100\text{ ms})$ versus E for different V^{2+} concentrations ranging from 0.5 to 3 mol %. These curves show two rising sections preceded and followed by linear portions whose common slope is practically equal to the differential capacity of the lipid monolayer in the absence of the viologen. The first Q versus E "wave" is 3 times higher than the second. The faradaic contribution $Q_f(t)$ to $Q(t)$ due to the reduction of V^{2+} is readily estimated by measuring the charge from the straight line obtained by extrapolation of the foot of the first wave (dashed curve in Figure 2); the extrapolated line practically coincides with the curve of the capacitive charge versus E as provided by the DOPC monolayer in the absence of V^{2+}. The maximum limiting value $Q_{f,max}$ attained by $Q_f(t)$

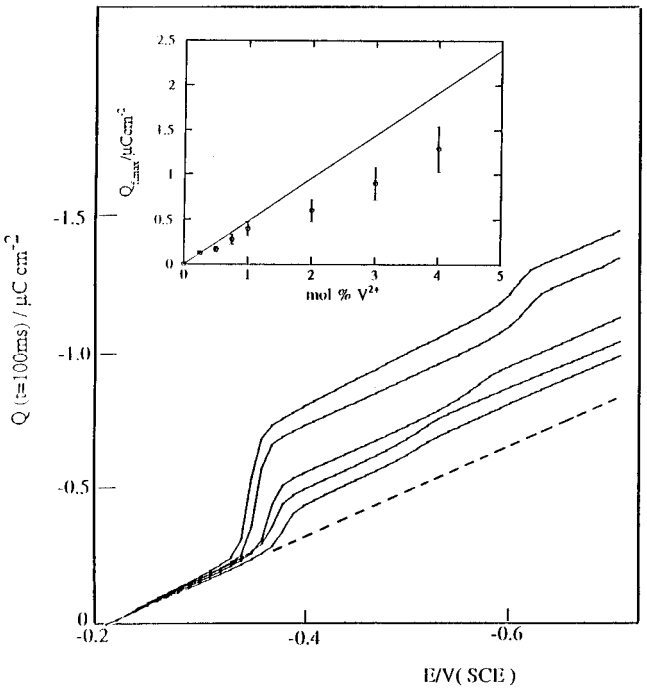

Figure 2. $Q(t{=}100\text{ms})$ versus E plots for V^{2+} electroreduction in aqueous 0.1 M KCl. From bottom to top, the V^{2+} concentrations in the DOPC monolayer are 0.50, 0.75, 1, 2, and 3 mol %. The dashed curve was obtained by extrapolating the foot of the $Q(t{=}100\text{ms})$ versus E curves. The inset shows a plot of $Q_{f,max}$ versus the V^{2+} concentration; the straight line is the charge for the complete two-electron reduction of V^{2+} to V^0 against E, estimated as described in the text.

is clearly independent of the electrolysis time t and measures the maximum charge involved in the reduction of the V^{2+} molecules incorporated in the film. The inset of Figure 2 shows a plot of $Q_{f,max}$ versus the V^{2+} concentration. At V^{2+} concentrations less than 1 mol % $Q_{f,max}$ is practically equal to the charge estimated for the complete two-electron reduction of V^{2+} to V^0 upon assuming that both the lipid and V^{2+} molecules occupy a surface area of 65 Å^2. Incidentally, at the low V^{2+} concentrations investigated the uncertainty in the actual surface area occupied by one V^{2+} molecule has an almost negligible effect on such an estimate. As the V^{2+} concentration is increased beyond 1 mol %, the $Q_{f,max}$ value starts to deviate from the estimated value, as appears from the inset of Figure 2. At V^{2+} concentrations higher than about 5 mol % experimental measurements become progressively more irreproducible; it is possible that at these high concentrations the V^{2+} molecules start to segregate into a separate phase, endangering the stability of the lipid monolayer.

The curves of the quadrature component of the admittance against the applied potential as obtained with V^{2+} incorporated in the DOPC film practically coincide with that for pure DOPC at potentials preceding and following the two waves of Figure 2, where the differential capacity C assumes a common value of about 1.75 μF cm^{-2}. As distinct from the behavior exhibited by ubiquinone-10 incorporated in a DOPC monolayer,[51] over the intermediate potential range covered by the two waves for V^{2+} electroreduction the quadrature component of the admittance shows a pronounced peak that increases with an increase in the V^{2+} concentration. Hence, in this case the equivalent circuit for the DOPC film with embedded V^{2+} cannot be simply regarded as consisting of a capacitance and a resistance in parallel.

A unitary increment in the logarithm of the V^{2+} concentration, Γ_2*, causes a shift in the half-wave potential $E'_{1/2}$ of the first wave by about 35 mV toward positive values and a concomitant

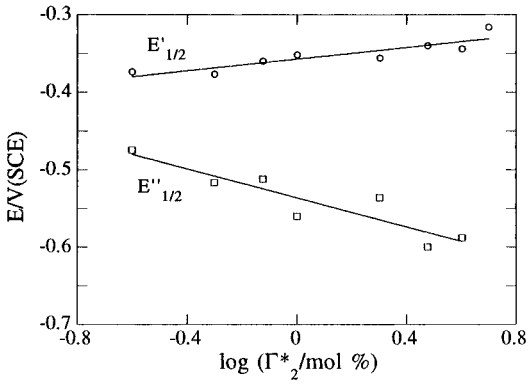

Figure 3. Plots of the half-wave potentials, $E'_{1/2}$ and $E''_{1/2}$, of the two consecutive waves for the electroreduction of V^{2+} incorporated in a DOPC monolayer, against log Γ^*_2.

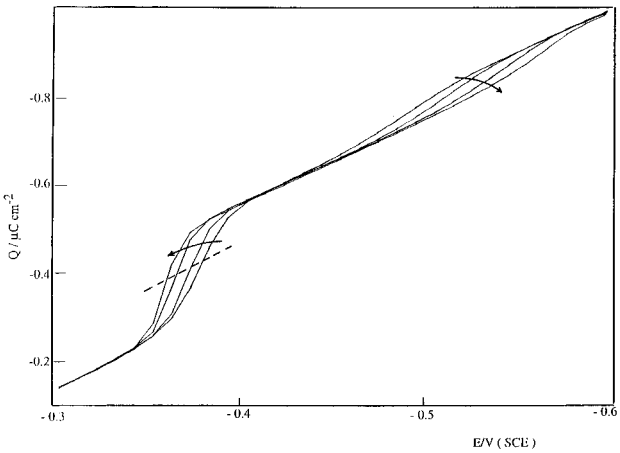

Figure 4. $Q(t)$ versus E curves at different electrolysis times t for the electroreduction of 1 mol % V^{2+} incorporated in a DOPC monolayer. t takes the values 10, 20, 50, and 100 ms in the direction of the two arrows. The dashed straight line corresponds to a faradaic charge $Q_f = -0.12$ μC cm^{-2}.

shift in the half-wave potential $E''_{1/2}$ of the second wave by about 90 mV in the negative direction, with a resulting increase in the separation between the two waves (see Figure 3). This separation also increases with increasing electrolysis time at constant Γ_2*. This is clearly apparent in Figure 4, which shows $Q(E)$ versus E curves for 1 mol % V^{2+} at different electrolysis times.

The charge density σ_M on the DOPC-coated mercury drop was measured both in the absence and in the presence of V^{2+} at three different potentials chosen along the foot and the plateaus of the two waves, i.e., at -0.25, -0.4, and -0.65 V. At these potentials and over the whole concentration range investigated the presence of V^{2+} was found to have no effect on the σ_M value within the accuracy of our measurements ($\sim$0.02 μC cm^{-2}). The major contribution to the potential difference across the interface is made by the potential difference across the hydrocarbon tail region of the lipid, which is approximately given by $4\pi(\sigma_M + \sigma_i)\beta/\epsilon_\beta$, where β and $\epsilon_\beta \approx 2$ are the thickness and the dielectric constant of this region and σ_i is the charge density due to any charged species directly adsorbed on the mercury surface. The fact that σ_M at constant applied potential does not change upon incorporation of V^{2+} implies that σ_i is very small and hence that the head groups of dioctadecylviologen and of the products of its partial electroreduction localize somewhere in the polar head region of the lipid monolayer.

The cyclic voltammogram of DOPC + V^{2+} shows a single reduction peak over the potential range of the first chronocou-

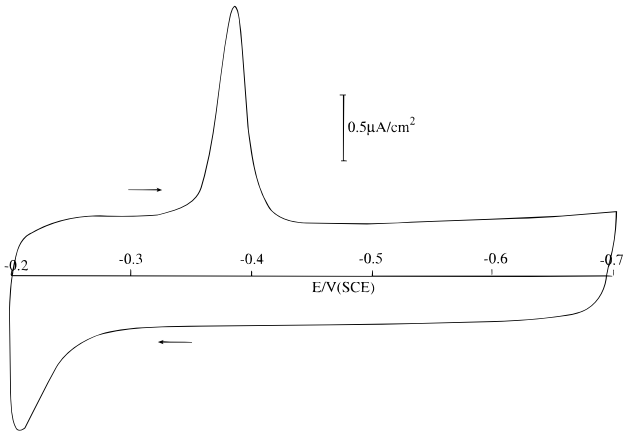

Figure 5. Cyclic voltammogram in aqueous 0.1 M KCl of 1 mol % V^{2+} incorporated in a DOPC-coated mercury electrode. Scan rate = 0.2 V s^{-1}.

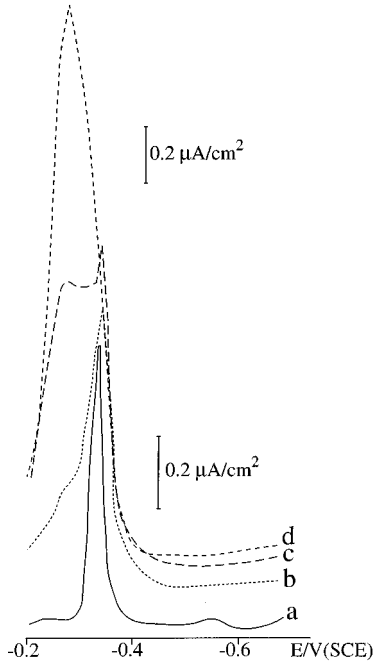

Figure 6. Differential pulse polarogram in aqueous 0.1 M KCl of 1 mol % V^{2+} incorporated in a DOPC-coated mercury electrode in the presence of 0 (a), 5×10^{-6} (b), 1×10^{-5} (c), and 4×10^{-5} M (d) ferricyanide. Scan rate = 7.5 mV s^{-1}; waiting period = 0.8 s; pulse height = 50 mV; pulse width = 0.2 s.

lometric wave, as shown in Figure 5. The anodic counterpart of this peak lies at potentials positive to −0.25 V, thus pointing to its pronounced irreversibility. To reproduce the cyclic voltammogram in Figure 5 by repeated cycling, a rest time of a few seconds at −0.2 V was required, to allow a complete reoxidation of the reduction product of V^{2+}. The differential pulse polarogram of DOPC + 1 mol % V^{2+} shows a sharp peak over the potential range of the first chronocoulometric wave, but only a hardly detectable hump at the potential of the second chronocoulometric wave (see curve a in Figure 6). The normal pulse polarogram of DOPC + 1 mol % V^{2+} in Figure 7 shows a sharp peak, which is unusual for this technique, at the potential of the rising portion of the first chronocoulometric wave, and a well-defined wave over the potential range of the second chronocoulometric wave.

Discussion

The plot of $Q_{f,max}$ versus the V^{2+} concentration having a slope corresponding to the uptake of 2 electrons per V^{2+} molecule (see the inset of Figure 2) up to 1 mol % V^{2+} strongly suggests that these molecules are intercalated in the DOPC monolayer; in fact, the presence of a separate "V^{2+} rich" phase would hardly allow a complete electroreduction of all the incorporated viologen in less than 1 ms. Moreover, this very rapid and complete electroreduction indicates that over the potential region covered by the two waves the translocation of V^{2+} is not rate-limiting, despite the fact that the electroactive moiety resides prevalently in the polar head region. Naturally, an electron tunneling across the hydrocarbon tail region cannot be excluded a priori, although it seems quite improbable. Thus, the height of the energy barrier across which the electron must tunnel decreases progressively as the difference between the applied potential E and the redox standard potential of the reducing species becomes more negative.[55] At a lipid-coated mercury electrode some evidence of electron tunneling is only observed with species such as Fe^{3+} and $Fe(CN)_6^{3-}$, whose overpotential is <-0.5 V (Moncelli, Herrero, and Guidelli, unpublished results). Conversely, the reduction peak potential for "bulk" dioctadecylviologen, as obtained by linear extrapolation of the experimental values for $(C_6)_2V^{2+}$, $(C_7)_2V^{2+}$, and $(C_8)_2V^{2+}$ (see Figure 8 of ref 25a), amounts to ~ -0.3 V/SCE.

A straightforward diagnostic criterion for the elucidation of the mechanism of an electroreduction process $O + ne \rightarrow R$ involving a well-defined amount of electroactive compound O directly adsorbed on the electrode surface or incorporated in a matrix coating the electrode consists in examining the relationship between applied potential E and electrolysis time t at constant faradaic charge Q_f by the chronocoulometric technique.[51,56] This procedure amounts to measuring the decrease in the electrolysis time required to produce the same surface concentration $\Gamma_R = Q_f/(nF)$ of product R starting from the same initial surface concentration Γ_O of reactant as a consequence of a negative shift in the applied potential. The state of affairs that is attained on the electrode surface after the flow of a constant faradaic charge Q_f is exactly the same at the various applied potentials. Hence, the relationship between E and t at constant Q_f is not affected by any dependence of the activity coefficients of the reacting species on the corresponding surface concentrations.

Figure 8 shows a plot of ln t versus $FE/(RT)$ over the t range from 10 to 100 ms, as obtained from Q versus E plots for the electroreduction of 1 mol % V^{2+} relative to different electrolysis times at a constant faradaic charge $Q_f = -0.12\ \mu C\ cm^{-2}$. This charge was chosen so as to lie along the rising portion of the first wave: it is represented by the dashed straight line in Figure 4, which shows a sample of the Q versus E curves employed for the plot of Figure 8. The latter plot is linear and exhibits a slope that is practically equal to 3. The same slope was obtained over the whole range of V^{2+} concentrations from 0.5 to 5 mol %.

A slope of ln t versus $FE/(RT)$ plots equal to 3 can be rationalized on the basis of the mechanism

$$V^{2+} + e \leftrightarrow V^{+} \quad (1a)$$

$$V^{+} + e \leftrightarrow V^{0} \quad (1b)$$

$$V^{+} + V^{0} \rightarrow V_2^{+} \quad (1c)$$

where the first two elementary charge transfer steps are in quasi equilibrium and the third one is a chemical rate-determining step. Electron transfer takes place quite probably when the electroactive moities of the V^{2+} and V^{+} species come into contact with the electrode surface. If this is the case, then the potential difference that affects electron transfer is smaller than

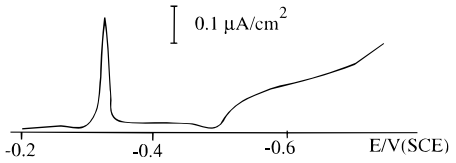

Figure 7. Normal pulse polarogram in aqueous 0.1 M KCl of 1 mol % V^{2+} incorporated in a DOPC-coated mercury electrode. Scan rate = 7.5 mV s^{-1}; initial potential $E_i = -0.2$ V; waiting period at $E_i = 3$ s; pulse width = 0.2 s.

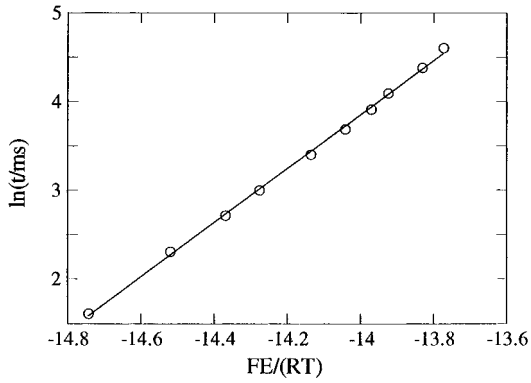

Figure 8. ln t versus $FE/(RT)$ plot as obtained at constant $Q_f = -0.12$ μC cm^{-2} from $Q(t)$ versus E curves relative to different electrolysis times t for the electroreduction of 1 mol % V^{2+} incorporated in a DOPC monolayer. The solid curve in the figure has a slope equal to 3.

the potential difference $\Delta\phi$ across the whole interface. However, any translocation of these electroactive moieties from the polar head region, where they preferentially reside, to the electrode surface must also be regarded as in quasi equilibrium. We can therefore apply the equilibrium conditions to the electron transfer steps of eqs 1a and 1b with the electroactive moieties located somewhere in the polar head region; upon assuming as a first approximation that the potential difference between the electrode surface $x = 0$ and the position of these moieties is practically equal to $\Delta\phi$, which in turn differs from the applied potential E by a constant depending exclusively on the choice of the reference electrode, we get

$$\Gamma_1/\Gamma_2 = K' \exp(-fE) \tag{2a}$$

$$\Gamma_0/\Gamma_1 = K'' \exp(-fE) \tag{2b}$$

with

$$K' \equiv \exp(fE'_0); \quad K'' \equiv \exp(fE''_0); \quad f \equiv F/(RT) \tag{3}$$

Here Γ_2, Γ_1, and Γ_0 are the concentrations of V^{2+}, V^+, and V^0 in the lipid monolayer, and E'_0 and E''_0 are the standard potentials of the redox couples V^{2+}/V^+ and V^+/V^0. Identical expressions would be obtained in the improbable case of electron tunneling steps in quasi equilibrium. The rate v of the coupling step (1c), which controls the overall process along the first wave, is given by

$$v = \frac{d\Gamma_{01}}{dt} = k\gamma_0\gamma_1\Gamma_0\Gamma_1 = kK'^2K''\gamma_0\gamma_1\Gamma_2^2 \exp(-3fE) \tag{4}$$

where Γ_{01} is the concentration of the V_2^+ dimer, γ_0, γ_1 are the activity coefficients of V^0 and V^+, and k is the rate constant of the coupling step. In writing this equation we have made use of eqs 2a and 2b. Integration of eq 4, in which $d\Gamma_{01}/dt$ is set equal to $-(1/2)(d\Gamma_2/dt)$, yields

$$\int_{\Gamma_2(t)}^{\Gamma^*_2} d\Gamma_2/(\gamma_0\gamma_1\Gamma_2^2) = 2kK'^2K'' \exp(-3FE)\, t \tag{5}$$

where Γ^*_2 is the initial surface concentration of V^{2+}. The integral on the left-hand side is constant at constant Q_f, since the concentration $\Gamma_2(t)$ and the activity coefficients γ_0 and γ_1 at a time t at which Q_f is constant are also constant. Hence, the same is true for the right-hand side, which therefore predicts a ln t versus $FE/(RT)$ plot with a slope equal to 3.

The mechanism of eq 1 is consistent with the presence of two $Q(t)$ versus E waves, the first of which is 3 times higher than the second. Since the overall height of the two waves corresponds to the uptake of two Faradays per mole of V^{2+}, the two consecutive waves involve the uptake of 3/2 and 1/2 of a Faraday, respectively. The processes responsible for the two waves are therefore

$$2V^{2+} + 3e \rightarrow V_2^+; \quad V_2^+ + e \rightarrow 2V_0$$

the first of which agrees with the mechanism of eq 1. This mechanism also explains the progressive separation of the two waves with an increase in Γ^*_2: the coupling step (1c) being proportional to the square of the viologen concentration causes an increase in Γ^*_2 to stabilize the dimer over the monomeric species and hence to broaden the intermediate potential region where the dimer predominates. Finally, the unusual flow of an anodic current following a negative potential jump, as observed in the first stages of electrolysis over the potential range of the second wave (see the descending portion of the $Q(t)$ versus t curves in Figure 1), can also be justified on the basis of the proposed mechanism. The potentials along the rising portion of the second wave are sufficiently negative to cause an almost instantaneous electroreduction of V^{2+} to V^0 on the electrode surface, but not so negative as to stabilize V^0 with respect to the V_2^+ dimer in the polar head region: V^0 is therefore partially reconverted to V_2^+ during the electrolysis at constant potential.

The dependence of the faradaic charge $Q_f(E,t)$ upon E and t according to the mechanism of eq 1 is obtained by taking into account the expression for the conservation of mass within the lipid monolayer:

$$\Gamma_2 + \Gamma_1 + \Gamma_0 + 2\Gamma_{01} = \Gamma^*_2 \tag{6}$$

The three algebraic relationships of eqs 2a, 2b, and 6 can be combined with eq 4, in which we will temporarily disregard the activity coefficients γ_0 and γ_1 for simplicity, to yield a simple differential equation in Γ_{01}; this is readily solved by separation of variables, giving the following expression for Γ_{01}:

$$\Gamma_{01} = \frac{Kkt\Gamma^{*2}_2}{1 + 2Kkt\Gamma^*_2} \quad \text{with}$$

$$K \equiv \frac{K'^2K'' \exp(-3fE)}{[1 + K' \exp(-fE) + K'K'' \exp(-2fE)]^2} \tag{7}$$

The faradaic charge $Q_f(t)$ is given by

$$Q_f(t) = \int_0^t i(t)\, dt = F\int_0^t \frac{d(\Gamma_1 + 2\Gamma_0 + 3\Gamma_{01})}{dt} dt = F(\Gamma_1 + 2\Gamma_0 + 3\Gamma_{01}) \tag{8}$$

Combining the algebraic equations (2a), (2b), and (6)−(8) yields the following expression of $Q_f(t)$ as a function of t, E, and Γ^*_2:

$$R \equiv \frac{Q_f}{F\Gamma^*_2} = \frac{1}{1+2K\tau}\left[3K\tau + \frac{K' \exp(-fE) + 2K'K'' \exp(-2fE)}{1 + K' \exp(-fE) + K'K'' \exp(-2fE)}\right] \quad \text{with} \quad \tau \equiv k\Gamma^*_2 t \quad (9)$$

For simplicity, in the following we will refer all potentials to the standard potential E'_0 of the redox couple V^{2+}/V^+, thus setting $E'_0 = 0$ and $K' = 1$.

Figure 9 shows a series of plots of R against the applied potential E for different pairs of values of τ and E''_0. These values were chosen in such a way as to produce a separation $\Delta E_{1/2} = E'_{1/2} - E''_{1/2}$ between the half-wave potentials of the two consecutive waves approximately equal to 0.22 V, which corresponds to the experimental separation for $\Gamma^*_2 = 2$ mol %. It can be seen that for E''_0 values more negative than about -0.20 V the stability of the V^+ species is high enough to produce three ill-defined consecutive waves corresponding to the processes $V^{2+} + e \rightarrow V^+$, $2V^+ + e \rightarrow V_2^+$, and $V_2^+ + e \rightarrow 2V^0$. As E''_0 is made less negative than -0.20 V, only two waves are predicted, the first of which has a slope that increases progressively until it attains a maximum for $E''_0 > -0.06$. This maximum slope can be measured by the value, 18.7 mV, of the difference, $E'_{1/4} - E'_{3/4}$, between the potentials corresponding to one-fourth and three-fourths of the limiting charge $Q_f = (3/2)F\Gamma^*_2$. This value is comparable with the experimental value of about 13 mV. This sets a minimum value of about -0.06 V for E''_0. Figure 10 shows a series of R versus t curves at different potentials E as calculated for $E''_0 = -0.02$ V and $k\Gamma^*_2 = 1.4 \times 10^3$ (s mol %)$^{-1}$. The curves account satisfactorily for the shape of the experimental $Q(t)$ versus t curves in Figure 1, including the unusual decrease of $Q(t)$ in time at the potentials corresponding to the second wave. Only the initial short "induction period" characterized by an almost horizontal portion of the experimental $Q(t)$ versus t curves in Figure 1 is not accounted for by the proposed mechanism.

The relatively large separation between the two waves permits the corresponding Q_f versus E characteristics to be expressed by distinct relationships to a good approximation. Thus, the first wave lies at potentials relatively positive to the reference potential E'_0 and hence unfavorable to the V^+ and V^0 species. The two species V^{2+} and V_2^+ will therefore decidedly predominate over the remaining two species along the rising portion of the first wave, allowing us to write eqs 6, 8, and 4 in the simplified forms

$$\Gamma_2 + 2\Gamma_{01} = \Gamma^*_2 \quad (10a)$$

$$R \equiv \frac{Q}{F\Gamma^*_2} = 3\frac{\Gamma_{01}}{\Gamma^*_2} \quad (10b)$$

$$-\frac{1}{2}\frac{d\Gamma_2}{dt} = kK''\Gamma_2^2 \exp(-3fE) \quad (10c)$$

Integrating the differential equation of eq 10c from $t = 0$, when $\Gamma_2 = \Gamma^*_2$, to a given time $t = t$ at which $\Gamma_2 = \Gamma_2$ and taking eqs 10a and 10b into account, we get

$$E = \frac{RT}{3F}\ln(2K''\tau) - \frac{RT}{3F}\ln\left(\frac{R}{3/2 - R}\right) \quad (11)$$

Noting that at the half-wave potential, $E'_{1/2}$, of the first wave R equals 3/4, from eq 11 it follows that

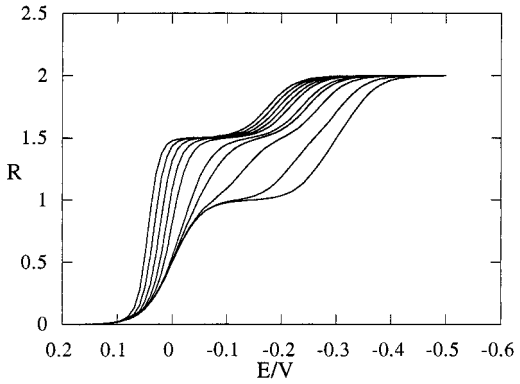

Figure 9. R versus E curves calculated for different pairs of values of τ and E''_0 chosen in such a way as to produce a separation $\Delta E_{1/2} \approx 0.22$ V. From left to right, the E''_0 values are -0.02, -0.04, -0.06, -0.08, -0.10, -0.14, -0.16, -0.20, -0.26, and -0.30 V; the corresponding values of $\tau \equiv k\Gamma^*_2 t$ are derived from eq 15.

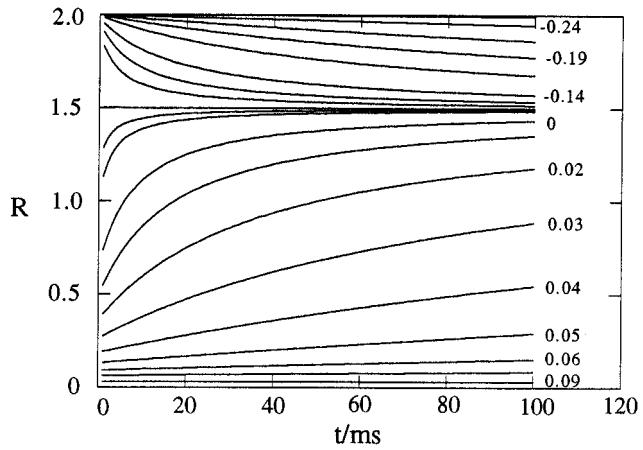

Figure 10. R versus t curves at different potentials E as calculated for $E''_0 = -0.02$ V and $k\Gamma^*_2 = 1.4 \times 10^3$ (s mol %)$^{-1}$. From bottom top, the E values are 0.09, 0.07, 0.06, 0.05, 0.04, 0.03, 0.02, 0.01, 0, -0.02, -0.03, -0.05, -0.10, -0.12, -0.14, -0.17, -0.19, -0.21, -0.24, and -0.30 V.

$$E'_{1/2} = \frac{RT}{3F}\ln(2K''k\Gamma^*_2 t) \quad (12)$$

This equation predicts a positive shift of $E'_{1/2}$ by 20 mV per each unitary increment of log Γ^*_2 at constant electrolysis time.

As opposed to the first wave, the second wave lies at potentials negative enough to the reference potential E'_0 as to favor the species V_0 and V_2^+ over the species V^{2+} and V^+. This permits us to simplify eqs 6, 8, and 4 as follows

$$\Gamma_0 + 2\Gamma_{01} = \Gamma^*_2 \quad (13a)$$

$$R \equiv \frac{Q}{F\Gamma^*_2} = \frac{2\Gamma_0 + 3\Gamma_{01}}{\Gamma^*_2} \quad (13b)$$

$$-\frac{1}{2}\frac{d\Gamma_0}{dt} = \frac{k}{K''}\Gamma_0^2 \exp(fE) \quad (13c)$$

The second wave covers the range of R values from 3/2 to 2. Hence, the half-wave potential $E''_{1/2}$ of this wave corresponds to $R = 3/2 + 1/4 = 7/4$. From eqs 13a and 13b it immediately follows that $\Gamma_0 = \Gamma^*_2/2$ at $E''_{1/2}$. Let us now integrate the differential equation of eq 13c from $t = 0$, when Γ_0 is practically equal to Γ^*_2 in view of the almost instantaneous conversion of V^{2+} into V^0, to a time t at which Γ_0 equals $\Gamma^*_2/2$ and hence E equals $E''_{1/2}$. We then obtain

$$E''_{1/2} = -(RT/F)\ln(2k\Gamma^*_2 t/K'') \quad (14)$$

This equation predicts a negative shift of $E''_{1/2}$ by 60 mV per each unitary increment of log Γ^*_2. From eqs 12 and 14 it follows that

$$\Delta E_{1/2} \equiv E'_{1/2} - E''_{1/2} = \frac{4RT}{3F}\ln\left(\frac{2k\Gamma^*_2 t}{K''^{1/2}}\right) = \frac{4RT}{3F}\ln(2k\Gamma^*_2 t) - \frac{2}{3}E''_0 \quad (15)$$

Hence, the separation between the two waves does not depend on $k\Gamma^*_2$ and E''_0 separately, but rather on their combination in eq 15. We already observed that the negative value of E''_0 cannot be <-0.06 V in view of the experimental value $\Delta E_{1/2} = 0.220$ V for $\Gamma^*_2 = 2$ mol % and $t = 0.1$ s and of the behavior of the calculated curves in Figure 9. Hence, from eq 15 it also follows that k cannot be <480 (s mol %)$^{-1}$.

The experimental shifts of $E'_{1/2}$ and $E''_{1/2}$ per each unitary increment of log Γ^*_2 amount to $\sim+35$ and ~-90 mV (see Figure 3), to be compared with the $+20$ and -60 mV values predicted by eqs 12 and 14. The percentage deviations from the predicted values are particularly significant for the first wave and should be ascribed to concentration dependent activity coefficients of the reacting species not accounted for in eqs 7−15. Here we will confine ourselves to considering the modifications to the treatment of eqs 10−12 for the first wave that are required to account for a coupling step taking place well inside the polar head region. In this case the potential difference that is operative in the electron transfer steps of eqs 1a and 1b as well as in the translocations from the electrode surface to the site of the coupling step is not the potential difference $\Delta\phi = (E + \text{const})$ across the whole interphase, but rather $\Delta\phi - 4\pi F(2\Gamma_2 + \Gamma_{01})\gamma/\epsilon_\gamma \equiv \Delta\phi - a(2\Gamma_2 + \Gamma_{01})$: here $F(2\Gamma_2 + \Gamma_{01})$ is the charge density at the site of the coupling step over the potential range of the first wave, γ is the "burial depth" of the V^{2+} and V_2^+ species in the polar head region, and ϵ_γ is the dielectric constant of this region. Incidentally, the replacement of E by $E - a(2\Gamma_2 + \Gamma_{01})$ does not invalidate the diagnostic criterion of eq 5, since Γ_2 and Γ_{01} are constant for a constant value of Q_f. Conversely, if we carry out this substitution in the differential equation of eq 10c and we integrate the resulting equation taking eq 10a into account, we get

$$2K''\tau\exp\left[-\frac{3F}{RT}\left(E - \frac{a\Gamma^*_2}{2}\right)\right] = \int_y^1 \exp\left(-\frac{9F}{2RT}a\Gamma^*_2 y\right)\frac{dy}{y^2} \equiv I(y) \quad \text{with} \quad y \equiv \frac{\Gamma_2}{\Gamma^*_2} \quad (16)$$

From eqs 10a and 10b it follows that

$$R \equiv \frac{Q}{F\Gamma^*_2} = \frac{3}{2}(1 - y) \quad (17)$$

At the half-wave potential, $E'_{1/2}$, of the first wave we have $R = 3/4$, and hence $y = 1/2$. $E'_{1/2}$ is therefore given by

$$E'_{1/2} = \frac{RT}{3F}\ln(2K''\tau) + \frac{a\Gamma^*_2}{2} - \frac{RT}{3F}\ln I(y{=}1/2) \quad (18)$$

The last two terms of this equation account for the deviations of $E'_{1/2}$ from the Γ^*_2 dependence expressed by eq 12 and are both functions of $(a\Gamma^*_2)/2$. Figure 11 shows a plot of $E'^*_{1/2} \equiv [E'_{1/2} - (RT/3F)\ln(4K''kt/a)]$ against $\log(a\Gamma^*_2/2)$. The figure

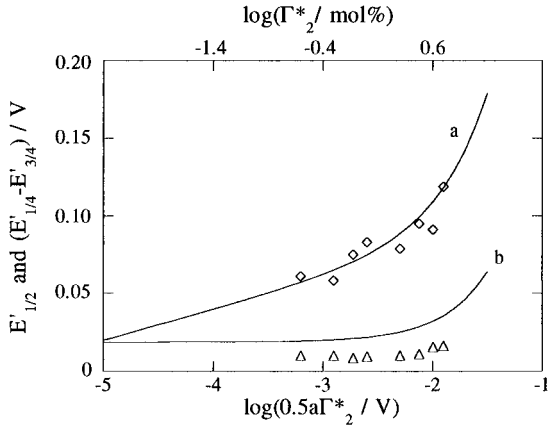

Figure 11. (Solid curves) Plots of $E'^*_{1/2}$ (a) and of $(E'_{1/4} - E'_{3/4})$ (b) against $\log(a\Gamma^*_2/2)$. The points are experimental values of $E'_{1/2}$ (◇) and of $(E'_{1/4} - E'_{3/4})$ (△) against $\log(\Gamma^*_2)$; the experimental $E'_{1/2}$ values have been translated along the vertical axis in order to attain the best overlapping on curve a.

also shows a plot of $(E'_{1/4} - E'_{3/4})$ as obtained from eq 16 by noting that at $E'_{1/4}$ and $E'_{3/4}$ the parameter R takes the values 3/8 and 9/8, and hence y takes the values 3/4 and 1/4 in view of eq 17. From Figure 11 it is apparent that the slope of the $E'_{1/2}$ versus $\log(a\Gamma^*_2/2)$ plot starts increasing rapidly with respect to the 20 mV value as $\log(a\Gamma^*_2/2)$ becomes > -3; this increase is accompanied by a concomitant decrease in the slope of the rising section of the first wave, as expressed by the $E'_{1/4} - E'_{3/4}$ value. Figure 11 also shows the best overlapping of the experimental $E'_{1/2}$ versus log Γ^*_2 plot on the calculated $E'^*_{1/2}$ versus $\ln(a\Gamma^*_2/2)$ plot, as obtained by translation of the experimental plot in both the horizontal and vertical directions. Comparing the horizontal axes of the experimental and calculated plots yields an a value of $\sim 5 \times 10^{-3}$ V/(mol %). If we estimate the surface area of a DOPC molecule at 65 Å^2, then a V^{2+} concentration of 1 mol % corresponds to 2.55×10^{-12} mol cm^{-2}, and the above a value corresponds to a γ/ϵ_γ ratio of 0.18 Å. If we ascribe to ϵ_γ the reasonable value of 20,[57] the burial depth γ amounts to 3.6 Å. Even though the experimental $E'_{1/4} - E'_{3/4}$ values are constantly smaller than the calculated ones, they start increasing in concomitance with the increase in the slope of the corresponding $E'_{1/2}$ versus log Γ^*_2 plot over 20 mV, in agreement with predictions.

The conclusions drawn from the chronocoulometric measurements agree with the response of the other electrochemical techniques. In this connection we must distinguish normal pulse polarography (NPP), where after each current sampling the applied potential is constantly stepped back to a potential at which V^{2+} is regenerated, from cyclic voltammetry (CV) and differential pulse polarography (DPP), where no such continuous regeneration takes place. Both the cyclic voltammogram of Figure 5 and the DP polarogram of Figure 6 indicate that at potentials close to -0.35 V an intermediate species is formed, which is sufficiently stable as not to be appreciably reduced further to V^0 at more negative potentials and is reoxidized irreversibly at potentials close to -0.2 V. This behavior contrasts with that expected for the intermediate monomeric cation radical V^+, which is normally found to behave either reversibly or quasi reversibly on mercury and is further reduced to V^0;[2] conversely, the present behavior points to some form of association. Moreover, the charge obtained by integrating the area under the single cyclic voltammetric peak for V^{2+} concentrations ≤ 1 mol % amounts to 3/2 of a Faraday per mole of reactant, pointing to the formation of the monocation dimer V_2^+, in agreement with the chronocoulometric results.

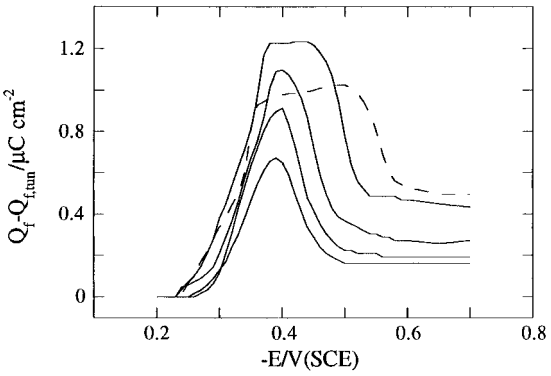

Figure 12. ($Q_f - Q_{f,tun}$) versus E plots for the electroreduction of V^{2+} incorporated in a DOPC-coated mercury electrode immersed in a solution of 0.1 M KCl + 5×10^{-5} M $K_3Fe(CN)_6$. Proceeding upward on the right-hand side of the figure, the V^{2+} concentrations in the DOPC monolayer are 0.5, 0.75, 1, 2, and 3.

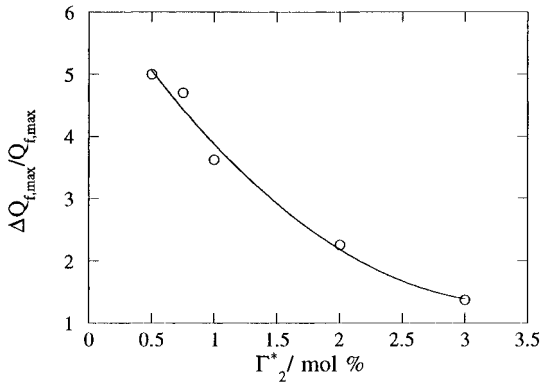

Figure 13. Plot of $\Delta Q_{f,max}/Q_{f,max}$ against Γ^*_2 as obtained from Figure 12.

As distinct from CV and DPP, the experimental conditions adopted in NPP are analogous to those used in chronocoulometry, the main difference being represented by the fact that the current is sampled at the end of each potential pulse, instead of being integrated during the whole pulse length. The presence of a current peak followed by a practically zero current in the NP polarogram of Figure 7 is therefore in agreement with the time independence of the chronocoulometric charge $Q(t)$ in Figure 1 for $t > 0.1$ s and -0.38 V $< E < -0.48$ V. The regular wave that develops at potentials negative to -0.5 V in Figure 7 indicates that V^{2+} can be reduced to its final reduction product V^0 only by stepping directly from a potential where V^{2+} is still electroinactive to one negative enough to stabilize the sole final reduction product V^0.

Evidence for some form of association of the cation radicals of various viologens, $RR'V^{2+}$ has been reported several times in the literature (for a review, see Bird and Kuhn[2]). In fact, as a class, one expects dimerization of these compounds. In principle, such dimers may be either monocation dimers, $R_2R'_2V_2^+$, or dication dimers, $R_2R'_2V_2^{2+}$.[2] The presence of dication dimers has often been postulated in protic media, although the association of these dimers with the corresponding inorganic anion has been suggested on grounds of electrostatic repulsion forces.[58,59] The predominance of the monocation dimer, V_2^+, of dioctadecylviologen in a medium of low dielectric constant and impermeable to inorganic anions, such as DOPC, is therefore justified.

Electron Transfer Mediation by V^{2+} from Aqueous Ferricyanide to Mercury across a DOPC Monolayer. A DOPC-coated mercury electrode is totally impermeable to ferricyanide at an applied potential of -0.2 V, even though on a bare mercury electrode this anion is reduced under diffusion-limiting conditions at the most positive potentials accessible on this metal. Nonetheless, a further negative shift in the potential E applied to a DOPC-coated mercury electrode in contact with an aqueous solution of $Fe(CN)_6^{3-}$ causes an increasing flow of a small but detectable faradaic charge $Q_{f,tun}(E)$ due to electron tunneling across the lipid monolayer. Incidentally, Tafel plots of ln $Q_{f,tun}(E)$ versus $-FE/(RT)$ are linear and yield a charge transfer coefficient $\alpha \approx 0.16$.

If V^{2+} is incorporated in the lipid monolayer, an appreciable excess ΔQ_f of faradaic charge over the sum of $Q_{f,tun}(E)$ plus the faradaic charge due to the reduction of V^{2+} alone is observed along the rising portion and the plateau of the first V^{2+} wave. This increase is clearly due to viologen acting as an electron transfer mediator between $Fe(CN)_6^{3-}$ and the mercury electrode. Figure 12 shows a number of $Q(E)$ versus E curves recorded at a mercury electrode coated with a DOPC film incorporating increasing amounts of V^{2+} and immersed in an aqueous solution of 0.1 M KCl + 5×10^{-5} M $Fe(CN)_6^{3-}$. Since the faradaic charge, $Q_{f,tun}(E)$, for $Fe(CN)_6^{3-}$ reduction due to tunneling and that due to electron transfer mediation by V^{2+} are expected to flow independently of each other, the curves in Figure 12 were reported after subtracting from the $Q(E)$ versus E curves obtained from DOPC + V^{2+} films in the presence of ferricyanide the curve obtained in the absence of V^{2+}: this yields the difference between the overall faradaic charge $Q_f(E)$ and $Q_{f,tun}(E)$. The excess faradaic charge ΔQ_f, as obtained upon subtracting from $Q_f(E) - Q_{f,tun}(E)$ the corresponding faradaic charge in the absence of ferricyanide, attains a maximum value at the beginning of the plateau of the first V^{2+} wave and then decreases progressively until it vanishes in the proximity of the rising portion of the second V^{2+} wave. In view of the process responsible for the second wave, we must discard the uncharged species V^0 as a possible electron transfer mediator from the electrode surface to the lipid/water interface. Figure 12 also shows that the excess faradaic charge $\Delta Q_{f,max}$ at the maximum of the $[Q_f(E) - Q_{f,tun}(E)]$ versus E curves increases with the V^{2+} concentration, Γ_2*, less than proportionally. This appears more clearly from the $\Delta Q_{f,max}/Q_{f,max}$ versus Γ_2* plot in Figure 13, where $Q_{f,max}$ is the limiting value of the faradaic charge as attained along the plateau of the second wave. Incidentally, $Q_{f,max}$ is unaffected by the presence of ferricyanide and measures the actual amount of V^{2+} incorporated in the lipid monolayer that is reduced almost instantaneously to V^0 at these negative potentials (see the inset of Figure 2). In view of the second-order coupling step of eq 1c, an increase in Γ_2* causes a progressive increase in the Γ_{01}/Γ_2* ratio and a concomitant decrease in the Γ_1/Γ_2* ratio at any given applied potential. Hence the trend in Figure 13 points unequivocally to V^+ as the reduced species acting as electron transfer mediator from the electrode surface to the lipid/water interface.

This conclusion is supported by the behavior of the DP polarograms of 1 mol % V^{2+} in the presence of increasing concentrations of ferricyanide, as shown in Figure 6: progressive additions of ferricyanide cause the appearance of a huge peak that develops at a potential about 80 mV more positive than the original peak, which ultimately disappears. This indicates that the species that mediates electron transport from ferricyanide to the mercury surface is not the one responsible for the peak in the absence of ferricyanide, i.e. V^{2+}, but rather a species that is formed at a slightly more positive potential, i.e. V^+.

Acknowledgment. The authors wish to thank Mr. Luciano Righeschi for valuable technical assistance. Thanks are due to the Universidad de la Coruña, Spain, for a fellowship to R.H. during the tenure of which the present results were obtained.

The financial support of the Ministero dell'Universita' e Ricerca Scientifica e Tecnologica and of the Consiglio Nazionale delle Ricerche is gratefully acknowledged.

References and Notes

(1) Ito, M.; Kuwana, T. *J. Electroanal. Chem*. **1971**, *32*, 415−425.
(2) Bird, C. L.; Kuhn, A. T. *Chem. Soc. Rev.* **1981**, *10*, 49−82.
(3) Steckhan, E.; Kuwana, T. *Ber. Bunsen.-Ges. Phys. Chem*. **1974**, *78*, 253−259.
(4) Szentrimay, P. Y.; Kuwana, T. In *Electrochemical Studies of Biological Systems*; Swayer, D., Ed.; American Chemical Society: Washington, DC, 1977; p 143.
(5) Hawkridge, F. M.; Kuwana, T. *Anal. Chem*. **1973**, *45*, 1021−1027.
(6) Landrum, H. L.; Salmon, R. T.; Hawkridge, F. M. *J. Am. Chem. Soc*. **1977**, *99*, 3154−3158.
(7) Stankovich, M. T. *Anal. Biochem*. **1980**, *109*, 295−308.
(8) Razumas, V. J.; Gudavicius, A. V.; Kulys, J. J. *J. Electroanal. Chem*. **1986**, *198*, 81−87.
(9) MacLachlan, K. L.; Crumbliss, A. L. *J. Electroanal. Chem*. **1990**, *296*, 113−122.
(10) Cotton, T. M.; Kim, J.-H.; Uphaus, R. A. *Microchem. J.* **1990**, *42*, 44−71.
(11) Feng, Q.; Yue, W.; Cotton, T. M. *J. Phys. Chem.* **1990**, *94*, 2082−91.
(12) Lu, T.; Cotton, T. M.; Hurst, J. K.; Thompson, D. H. P. *J. Phys. Chem.* **1988**, *92*, 6978−85.
(13) De Long, H. C.; Buttry, D. A. *Langmuir* **1990**, *6*, 1319−1322.
(14) Lee, C.-W.; Bard, A. J. *J. Electroanal. Chem.* **1988**, *239*, 441−446.
(15) Bunding-Lee, K. A. *Langmuir* **1990**, *6*, 709−712.
(16) Widrig, C. A.; Majda, M. *Langmuir* **1989**, *5*, 689−695.
(17) Yasuda, A.; Kondo, H.; Itabashi, M.; Seto, J. *J. Electroanal. Chem*. **1986**, *210*, 265−275.
(18) For a review, see: Cotton, T. M.; Kim, J.-H.; Uphaus, R. A. *Microchem. J.* **1990**, *42*, 44−71.
(19) Diaz, A.; Quintela, P. A.; Schuette, J. M.; Kaifer, A. E. *J. Phys. Chem.* **1988**, *9*, 3537−3542.
(20) Kaifer, A. *J. Am. Chem. Soc.* **1986**, *108*, 6837−6838.
(21) Lu, T.; Cotton, T. M.; Hurst, J. K.; Thompson, D. H. P. *J. Electroanal. Chem.* **1988**, 246−337.
(22) Garcia, O. J.; Quintela, P. A.; Kaifer, A. E. *Anal. Chem.* **1989**, *61*, 979−981.
(23) Van Dam, H. T.; Ponjee, J. J. *J. Electrochem. Soc.* **1974**, *121*, 1555−1558.
(24) Diaz, A.; Kaifer, A. E. *J. Electroanal. Chem.* **1988**, *249*, 333−338.
(25) Kitamura, F.; Ohsaka, T.; Tokuda, K. *J. Electroanal. Chem*. (a) **1993**, *347*, 371−381; (b) **1993**, *353*, 323−328; (c) **1994**, *368*, 281−284.
(26) Bae, I. T.; Huang, H.; Yeager, E. B.; Scherson, D. A. *Langmuir* **1991**, *7*, 1558−1562.
(27) Kokkinidis, G.; Hasiotis, C.; Papanastasiou, G. *J. Electroanal. Chem*. **1993**, *350*, 235−249.
(28) Li, J.; Kaifer, A. E. *Langmuir* **1993**, *9*, 591−596.
(29) Lee, C.; Kim, C.; Park, J. W. *J. Electroanal. Chem*. **1994**, *374*, 115−121.
(30) De Long, H. C.; Buttry, D. A. *Langmuir* **1992**, *8*, 2491−2496.
(31) Yamada, K.; Lin, C. B.; Kobayashi, N.; Ikeda, K.; Hirohashi, R.; Kaneko, M. *J. Electroanal. Chem*. **1994**, *370*, 59−65.
(32) Redepenning, J.; Miller, B. R.; Burnham, S. *Anal. Chem*. **1994**, *66*, 1560−1565.
(33) Lapkowski, M.; Bidan, G. *J. Electroanal. Chem*. **1993**, *362*, 249−256.
(34) Fujihira, M.; Araki, T. *Bull. Chem. Soc. Jpn.* **1986**, *59*, 2375−2379; *J. Electroanal. Chem.* **1986**, *205*, 329−333.
(35) Thompson, D. H. P.; Barrette, W. C., Jr.; Hurst, J. K. *J. Am. Chem. Soc*. **1987**, *109*, 2003−2009.
(36) Patterson, B. C.; Hurst, J. K. *J. Chem. Soc*. **1990**, *17*, 1137−1138.
(37) Lei, Y.; Hurst, J. K. *J. Phys. Chem.* **1991**, *95*, 7918−7925.
(38) Lymar, S. V.; Hurst, J. K. *J. Am. Chem. Soc.* **1992**, *114*, 9498−9503.
(39) Patterson, B. C.; Hurst, J. K. *J. Phys. Chem*. **1993**, *97*, 454−465.
(40) Kuhn, E. R.; Hurst, J. K. *J. Phys. Chem*. **1993**, *97*, 1712−1721.
(41) Lymar, S. V.; Hurst, J. K. *J. Phys. Chem*. **1994**, *98*, 989−996.
(42) Hammarström, L.; Almgren, M.; Lind, J.; Merényi, G.; Norrby, T.; Åkermark, B. *J. Phys. Chem*. **1993**, *97*, 10083−10091.
(43) Hammarström, L.; Berglund, H.; Almgren, M. *J. Phys. Chem*. **1994**, *98*, 9588−9593.
(44) Hammarström, L.; Almgren, M. *J. Phys. Chem*. **1995**, *99*, 11959−11966.
(45) Han, M.; Kaifer, A. E. *J. Chem. Soc., Chem. Commun.* **1990**, *23*, 1698−1701.
(46) Miller, I. R. In *Topics in Bioelectrochemistry and Bioenergetics*; Milazzo, G., Ed.; Wiley: Chichester, 1981; pp 194−225.
(47) Nelson, A.; Benton, A. *J. Electroanal. Chem*. **1986**, *202*, 253−270.
(48) Moncelli, M. R.; Becucci, L.; Guidelli, R. *Biophys. J.* **1994**, *66*, 1969−19852.
(49) Moncelli, M. R.; Becucci, L. *J. Electroanal. Chem*. **1995**, *385*, 183−189.
(50) Moncelli, M. R.; Herrero, R.; Becucci, R.; Guidelli, R. *J. Phys. Chem*. **1995**, *99*, 9940−9951.
(51) Moncelli, M. R.; Becucci, L.; Nelson, A.; Guidelli, R. *Biophys. J.* **1996**, *70*, 2716−2726.
(52) Foresti, M. L.; Moncelli, M. R.; Guidelli, R. *J. Electroanal. Chem.* **1980**, *109*, 1−14.
(53) Carlà, M.; Sastre de Vicente, M.; Moncelli, M. R.; Foresti, M. L.; Guidelli, R. *J. Electroanal. Chem*. **1988**, *246*, 283−296.
(54) Becucci, L.; Moncelli, M. R.; Guidelli, R. *J. Electroanal. Chem.* **1996**, *413*, 187−193.
(55) Lipkowski, J.; Buess-Hermann, Cl.; Lambert, J. P.; Gierst, L. *J. Electroanal. Chem*. **1986**, *202*, 169−189.
(56) Sastre de Vicente, M.; Moncelli, M. R.; Guidelli, R. *J. Electroanal. Chem*. **1988**, *248*, 55−67.
(57) Flewelling, R. F.; Hubbell, W. L. *Biophys. J.* **1986**, *49*, 541−552.
(58) Vargalyuk, V. F.; Starokozheva, T. I.; Loshkarev, Yu. M.; Savel'eva, N. Ya. *Elektrokhimiya* **1979**, *15*, 238−241.
(59) Vargalyuk, V. F.; Starokozheva, T. I.; Loshkarev, Yu. M. *Electrokhimiya* **1979**, *15*, 1551−1553.